Limnol. Oceanogr., 58(4), 2013, 1491–1500

doi:10.4319/lo.2013.58.4.1491

Depth distribution of ammonia oxidation rates and ammonia-oxidizer community composition in the Sargasso Sea

Silvia E. Newell,[a,*] Sarah E. Fawcett, and Bess B. Ward

Department of Geosciences, Princeton University, Princeton, New Jersey

Abstract

Ammonia oxidation rates and ammonia-oxidizer community structure were examined in a depth profile (20–2000 m) at the Bermuda Atlantic Time-Series Study site in December 2009. Ammonia oxidation rates, measured from trace additions of $^{15}NH_4^+$ (12–18 nmol L^{-1}), ranged from undetectable at the surface and 2000 m to 2.0 ± 0.1 nmol L^{-1} d^{-1} at 120 m, the depth of the primary nitrite maximum (PNM). Nitrification was not detectable in the photic zone in December, perhaps in part due to the density structure of the upper water column at this time. Ammonium oxidation rates varied with ammonium concentration and yielded an estimate for the half-saturation constant of 65 ± 41 nmol L^{-1} for the assemblage at 100 m. This value is similar to that reported for the cultivated marine ammonia-oxidizing archeon *Nitrosopumilus maritimus* (134 nmol L^{-1}), confirming the high affinity for ammonium of the in situ community in the Sargasso Sea. Ammonia-oxidizing archaeal (AOA) *amoA* gene copy numbers were two orders of magnitude higher than ammonia-oxidizing bacterial (AOB) *amoA* gene copy numbers at the PNM depth, suggesting that AOA were responsible for most of the ammonium oxidation, which was in turn responsible for the formation of the PNM. AOB abundance exceeded AOA at depths below 140 m, where both groups were much less abundant. Application of an AOA *amoA* functional gene microarray showed a diverse and even community distribution. A single archetype (AOA24, representing sequences originally from a coral reef) had the highest fluorescence ratio at depths of 0–1000 m.

Nitrification is the ultimate source of nitrate that supports phytoplankton growth in the surface ocean, whether the nitrate is mixed up from deep waters or produced in the euphotic zone. Ammonia oxidation to nitrite is the first step of nitrification, long thought to be mediated by ammonia-oxidizing bacteria (AOB). However, within the last decade, ammonia-oxidizing archaea (AOA) have also been confirmed as active ammonia oxidizers (Konnecke et al. 2005) and were found to be widespread (Francis et al. 2005) and abundant (Church et al. 2010) in the marine environment.

Although the discovery of AOA has recentered attention on nitrification in marine environments, there are still few direct measurements of both ammonia oxidation rates and ammonia-oxidizer gene abundance in the ocean. It is therefore difficult to quantify the contribution of nitrification to total primary production on a global scale (Yool et al. 2007). Additionally, the role of nitrifiers in forming the primary nitrite maximum (PNM) and the extent to which they compete with phytoplankton for ammonium is not well understood (Lomas and Lipschultz 2006). The highest rates of ammonium oxidation seem to correlate with the greatest concentrations of nitrite (i.e., at the PNM; Ward et al. 1982; Beman et al. 2008; Newell et al. 2011), but nitrite can also be produced by phytoplankton during reduction of nitrate such that the relative importance of these two processes in maintaining the PNM has become a subject of debate (Kiefer et al. 1976; Lomas and Lipschultz 2006; Mackey et al. 2011). Similarly, there are few studies clearly linking environmental factors beyond salinity (Francis et al. 2003; Bernhard et al. 2007, 2009) to controls on AOA and AOB community composition and distribution. Indeed, a recent study, Bouskill et al. (2011) showed inconsistent relationships with oxygen, ammonium, and nitrite across marine environments.

Abundances of AOB and AOA are commonly evaluated using quantitative polymerase chain reaction (PCR) analysis of the key functional gene, *amoA*. In general, AOA *amoA* genes appear to outnumber AOB *amoA* genes in open ocean environments (Wuchter et al. 2006; Mincer et al. 2007; Santoro et al. 2010). A potential explanation for the marine AOA dominance could be their high substrate affinity compared to AOB, as suggested by Martens-Habbena et al. (2009) from their work on *Nitrosopumulis maritimus*. However, the substrate affinity of natural assemblages of AOA is not well characterized, so whether *N. maritimus* is representative of the wider marine AOA population is unknown. Evidence for a high substrate affinity of the total in situ ammonia-oxidizer community was shown by Ward and Kilpatrick (1990). Using tracer experiments to measure ammonia oxidation rates, they observed no response of nitrification rate to ammonium concentration, implying that the half saturation constant (K_m) of the in situ assemblage was < 200 nmol L^{-1}.

The diversity of the global AOA community is often investigated using the *amoA* gene sequence. The database of AOA *amoA* sequences has grown rapidly, and it appears that the AOA *amoA*, like the AOB *amoA*, is less diverse than other functional genes (e.g., *nirS* [Francis et al. 2003; Dang et al. 2008, 2009] and *nifH* [Dang et al. 2013]). Analysis of clone libraries is useful for investigating further diversity, but it is time consuming, whereas the use of high-throughput functional gene microarrays is a far more efficient approach

* Corresponding author: sen@bu.edu

[a] Present address: Department of Earth and the Environment, Boston University, Boston, Massachusetts

for characterizing the distribution of known sequence types (Ward et al. 2007; Bouskill et al. 2011).

The Bermuda Atlantic Time-Series Study (BATS) site in the Sargasso Sea has been the location of extensive research over the last 30 yr, providing a rich contextual geochemical and biological database for new research (Lomas et al. in press). The oligotrophic conditions characteristic of the late summer and fall at BATS are representative of the ocean's largest biome, the subtropical gyres. June through December is considered the "oligotrophic period" (Lipschultz 2001), during which the nitrate supply to the euphotic zone (upper $\sim$ 100 m) is assumed to be impeded (Menzel and Ryther 1960; Lipschultz 2001; Steinberg et al. 2001). During this time, the two primary sources of "new" nitrogen to surface waters are thought to be injections of subsurface nitrate via the passage of mesoscale eddies, introducing 0.19–0.35 mol N m^{-2} yr^{-1} (McGillicudy et al. 1998), and nitrogen fixation, estimated to produce 0.072 mol N m^{-2} yr^{-1} (Gruber and Sarmiento 1997). The nitrate concentration is usually $\leq$ 10 nmol L^{-1} throughout the euphotic zone during the oligotrophic period, and ammonium concentrations are variable throughout the year, ranging from $<$ 10 nmol L^{-1} to sporadic observations $>$ 80 nmol L^{-1} (Lipschultz et al. 1996; Lipschultz 2001). Recent work has shown that in December 2009, when our experiments were conducted, the sole N source to all phytoplankton throughout the euphotic zone at BATS was recycled N (predominantly NH_4^+; Fawcett 2012).

There are few reported nitrification rates from the BATS site, and most of those that do exist have been calculated or measured indirectly. Lipschultz et al. (1996) calculated nitrite turnover rates of 3–7 d from a 3-yr time series of nitrite concentrations at BATS in the 150–1000 m depth interval (which often included the PNM). This turnover rate implies a nitrification rate of about 1 nmol L^{-1} d^{-1}. Lomas et al. (2009) reported no detectable nitrification between 0 and 220 m during the late winter using a nitrate isotope dilution method, whereas Lipschultz (2001) did detect nitrification at depths shallower than 150 m in August, also from isotope dilution experiments. During the late spring bloom at BATS, Beman et al. (2011) measured an ammonia oxidation rate of 16 nmol L^{-1} d^{-1} at 150 m from ammonium tracer incubations. Although these rates are lower than those reported for higher-nutrient environments, nitrification may also play an important role in the euphotic zone at BATS. Indeed, a modeling study calculated that 55% of the annual nitrate consumed by phytoplankton at BATS could derive from nitrification in the upper 200 m (Martin and Pondaven 2006).

The purpose of the present study was to determine the depth distribution of ammonia oxidation rates and ammonia-oxidizer community structure at BATS and to assess the affinity of the natural assemblage for ammonia. We hypothesized that (1) the ammonia oxidation rates would be low but that detectable rates would be associated with the PNM, (2) the AOA *amoA* gene would be more abundant than the AOB *amoA* gene, and (3) AOA genotypes would be biogeographically consistent: that is, the most abundant groups observed in other oligotrophic environments would also dominate at BATS.

Methods

Sample collection—Samples were collected from eight depths (20, 60, 80, 100, 120, 140, 1000, and 2000 m) aboard the R/V *Atlantic Explorer* on BATS cruise B253 at the BATS site (31°40′N, 64°10′W) on 10 December 2009 using a SeaBird conductivity temperature depth (CTD) and Niskin rosette. At each depth, duplicate 500 mL gas- and light-impermeable, trace metal–clean trilaminate bags were filled. Each bag was injected with 12–18 nmol L^{-1} $(^{15}NH_4)_2SO_4$ (as NH_4^+) plus 127–193 nmol L^{-1} carrier $Na^{14}NO_2^-$ (for final concentrations, *see* Table 1) while being filled directly from the Niskin bottles. After filling, 45 mL initial (T_0) samples were removed from each bag and frozen. Bags were incubated at near in situ temperature for approximately 12 h, after which 45 mL final (T_f) samples were removed and frozen.

After the bags were filled, water remaining in the Niskin bottles was emptied into 4 liter dark bottles, filtered onto 0.2 μm pore size Sterivex capsules, frozen immediately in liquid nitrogen, and transported back to the laboratory for deoxyribonucleic acid (DNA) analysis.

Nutrient methods—Seawater was collected for measurement of nitrate (NO_3^-), nitrite (NO_2^-), and ammonium (NH_4^+) concentrations from the surface to 1500 m. Samples were collected directly from the Niskin bottles into 60 mL high-density polyethylene (HDPE) acid-washed Nalgene bottles and immediately frozen at -20°C for later analysis in the laboratory.

Water column nitrate concentrations—Seawater samples were analyzed for nitrate concentration ($[NO_3^-]$) using a "NoxBox" (Teledyne model no. 200 EU). $[NO_3^-]$ was determined by injecting 100–1000 μL of seawater sample into a 90°C acidic solution of vanadium (V[III]; Braman and Hendrix 1989; Garside 1982) in a configuration with a detection limit of $\sim$ 0.02 μmol L^{-1}. This measurement includes nitrite (NO_2^-), which was measured independently (*see* below) and then subtracted to yield a value for $[NO_3^-]$ only.

Water column nitrite concentrations—Seawater samples were analyzed for nitrite concentrations ($[NO_2^-]$) according to the colorimetric method of Strickland and Parsons (1968). Briefly, 10 mL of sample was aliquoted into 12 mL combusted glass Wheaton vials to which 200 μL of both sulfanilamide and N-1-naphthyleneethylenediamine was added. Standards ranging in concentration from 0 to 200 nmol L^{-1}, made by diluting a high-concentration $NaNO_2$ stock solution with NO_2^--free seawater, were treated in the same way as the samples. Absorbance (543 nm) was measured using a Varian 100 Bio Ultra Violet-Visible Spectrophotometer equipped with a 10 cm path-length cuvette.

Water column ammonium concentrations—The ammonium concentration ($[NH_4^+]$) of surface samples was measured according to the method of Holmes et al. (1999). Briefly, 20 mL of sample was aliquoted into 30 mL acid-washed

Table 1. Ammonia oxidation rate experiment.

Depth (m)	Sample volume (liters)	$^{15}NH_4^+$ addition (nmol L^{-1})	Final $^{15}NH_4^+$ concentration (nmol L^{-1})	Carrier $^{14}NO_2^-$ addition (nmol L^{-1})	Incubation temperature (°C)
20	0.48	14.6	40.8	156.8	23.6
20	0.44	15.9	42.1	171.0	23.6
60	0.49	14.3	23.5	153.6	23.6
60	0.49	14.3	23.5	153.6	23.6
80	0.54	13.0	19.7	139.4	23.6
80	0.44	15.9	22.6	171.0	23.6
100	0.58	12.1	20.2	129.7	23.6
100	0.59	11.9	20.0	127.5	23.6
120	0.48	14.6	22.3	156.8	23.6
120	0.39	17.9	25.6	192.9	23.6
140	0.42	16.7	38.3	179.2	23.6
140	0.44	15.9	37.5	171.0	23.6
1000	0.43	16.3	16.3	175.0	4
1000	0.39	17.9	17.9	192.9	4
2000	0.43	16.3	16.3	175.0	4
2000	0.43	16.3	16.3	175.0	4

HDPE bottles, which had been rinsed copiously with NH_4^+-free seawater. From each depth, at least two different samples (sometimes from multiple Niskin bottles) were analyzed. Standards ranging in concentration from 0 to 200 nmol L^{-1} were made by diluting a high concentration NH_4Cl stock solution with NH_4^+-free seawater that was collected from 1000 m in the Sargasso Sea in order to ensure that the standard matrix was as similar as possible to that of the samples. Five milliliters of working reagent (orthophthaldialdehyde, sodium sulfite, and sodium borate) was added to both the standards and the samples, which were left in the dark at room temperature for 3 h before fluorescence was measured using a Trilogy fluorometer (Turner Designs, model no. 7200-000, with chromophoric dissolved organic matter NH_4 filter, model no. 7200-041). NH_4^+ standards were measured before and after the samples to account for any variation in fluorescence with time, which was found to be insignificant.

Analysis of $^{15}NO_2^-$—The sodium azide method of McIlvin and Altabet (2005) was used to convert NO_2^- to N_2O for ^{15}N analysis. In brief, a buffer of 1:1 by volume mixture of 20% acetic acid and 2 mol L^{-1} sodium azide was purged with He at 1.38×10^5 Pa for 10 min. The azide acetic acid buffer (0.30 mL) was added to 7.5 mL sample aliquots in 12 mL Exetainer vials (LabCo) and shaken vigorously. After 15 min, 0.15 mL of 6 mol L^{-1} NaOH was added, and the vial was shaken. All reactions were performed at room temperature in a fume hood.

Samples were shipped inverted to the University of California Davis Stable Isotope Facility, where N_2O concentrations and $^{45/44}N_2O$ isotope ratios were measured using a SerCon Cryoprep trace gas concentration system interfaced to a PDZ Europa 20-20 isotope ratio mass spectrometer (Sercon). The detection limit for isotopic measurements was 1 nmol N_2O, and blanks were air N_2. $^{46}N_2O$ was not detected at levels significantly above background in any sample. Rate measurements were calculated from the production of $^{45}N_2O$ (converted from $^{15}NO_2^-$) from the $^{15}NH_4^+$ tracer additions after subtracting any $^{15}NO_2^-$ and ambient $^{45}N_2O$ in the T_0 sample. Any $^{15}NO_2^-$ produced during the 12 h incubation was assumed to have resulted from ammonia oxidation. Nitrification rates were calculated using the equations of Ward and Kilpatrick (1990) without accounting for ammonium regeneration. The rates calculated from the production of $^{15}NO_2^-$ over 24 h were adjusted to account for less than 100% labeling of the in situ ammonium pool (Beman et al. 2011).

Quantitative PCR analysis—Quantitative PCR (qPCR) assays followed the method of Newell et al. (2011). Briefly, primers Arch-amoAF and Arch-amoAR (Francis et al. 2005) were used to amplify a 635 base-pair (bp) region of archaeal *amoA* for qPCR. Primers amoAF and amoA2R (Rotthauwe et al. 1997) were used to amplify a 491 bp region of β-AOB *amoA*. Standards for quantification of both AOB and AOA *amoA* were prepared by amplifying a constructed plasmid containing the respective *amoA* gene fragment, followed by quantification and serial dilution.

AOA or AOB *amoA* assays for all depths were carried out within a single assay plate (Smith et al. 2007). Each assay included triplicates of the no template controls, the three standards, and the environmental DNA samples. For the qPCR amplification mixture, the Quantitect SYBR Green PCR kit (Qiagen) was used. DNA was quantified using a NanoDrop ND-1000 spectrophotometer (NanoDrop Technologies), and 20–25 ng of template were amplified in each reaction carried out on a Stratagene MX3000P (Agilent Technologies). AOA *amoA* amplification followed the protocol of Francis et al. (2005), and β-AOB *amoA* amplification followed the protocol of Beman et al. (2008). Automatic analysis settings were used to determine the threshold cycle (Ct) values. The gene copy numbers were calculated according to

$$\text{gene copy number} = (\text{ng} \times \text{number mol}^{-1})/(\text{bp} \times \text{ng g}^{-1} \times \text{g mol}^{-1}\ \text{of bp})$$

and then converted to gene copy number per milliliter of seawater filtered, assuming 100% extraction efficiency.

AOA microarray analysis—The array (BC015) was developed following the archetype array approach described and employed previously (Bulow et al. 2008; Ward and Bouskill 2011) with 90 mer oligonucleotide probes. Each probe included an AOA *amoA*-specific 70 mer region and 20 mer control region (5′-GTACTACTAGCCTAGGCTAG-3′) bound onto a glass slide. The design and spotting of the *amoA* probes has been described previously (Ward et al. 2007). The 31 AOA archetype probes represent ~ 2000 sequences from a wide range of environments. The probe accession numbers and sequences have been reported previously (Bouskill et al. 2011).

Target preparation microarray hybridization and data analysis—Array analysis was performed as described previously (Ward and Bouskill 2011). Hybridization targets were prepared from gel-extracted and cleaned AOA *amoA* qPCR products (Qiagen). Briefly, the cleaned products were labeled with an amino-allyl-dUTP (Ambion) during linear amplification using random octamers and a Klenow polymerase (Applied Biosystems). The reaction contained 3.9 mmol L^{-1} d(AGC)TP, 0.4 mmol L^{-1} dTTP, and 4.8 mmol L^{-1} dUaa and was amplified for 3 h at 37°C. The Klenow product was purified and conjugated with Cy3. The Cy3-labeled target (200 ng) was combined with 2× hybridization buffer (1× final concentration; Agilent) and 0.25 pmol of a Cy5-labeled complementary 20 mer standard oligonucleotide and incubated at 95°C for 5 min before being cooled to room temperature. Targets were hybridized to duplicate arrays by overnight incubation at 65°C and then washed. The arrays were scanned with a laser scanner (Molecular Devices 4300) and analyzed with Gene Pix Pro 6.0 software (Molecular Devices). The ratio of Cy3 to Cy5 fluorescence intensities was standardized to the highest Cy3-to-Cy5 fluorescence ratio across the AOA probe set (normalized fluorescence ratio, FRn) to allow comparison across arrays (Bulow et al. 2008). Quality control was employed to remove noise by eliminating features in which the Cy3 signal was not at least twice the value of the control probes and the Cy3 : Cy5 was not at least 1% of the total *amoA* signal from all 31 probes. All of the original array data are available at Gene Expression Omnibus (GEO; http://www.ncbi.nlm.nih.gov/projects/geo) at the National Center for Biotechnology Information under GEO accession no. GSE422867.

Kinetics of ammonia oxidation—To investigate the dependence of ammonia oxidation rate on substrate concentration, eight bags were filled with seawater from 100 m. Each set of two bags received a different concentration of $^{15}NH_4^+$ tracer (ranging from 1.8 to 248 nmol L^{-1}) and 150–200 nmol L^{-1} carrier $^{14}NO_2^-$ (Table 2). The bags were sampled and analyzed for ammonium concentration and ammonia oxidation rate as described above.

To estimate the affinity (K_m) of the ammonia oxidizers for ammonia, as well as the community's maximum oxidation rate (V_{max}), measured ammonia oxidation rates at similar substrate concentrations were paired, and the mean ± standard deviation (SD) was calculated for each pair. Assuming a Gaussian distribution for the rate pairs, a Monte Carlo approach was used to generate 100,000 likely rates for each substrate concentration. Given that $^{15}NH_4^+$ tracer was added in uneven increments during the kinetic experiment (Table 2), the Eadie–Hofstee linearization is most appropriate for estimating K_m and V_{max}; 100,000 estimates of K_m and V_{max} were thus computed, from which the mean ± SD for each parameter was calculated. Using these mean values, a Michaelis–Menten function was fit to the ammonium concentration and oxidation rate data.

Table 2. Kinetic rate experiment at 100 m.

Sample volume (L)	$^{15}NH_4^+$ addition (nmol L^{-1})	Final $^{15}NH_4^+$ concentration (nmol L^{-1})	Carrier $^{14}NO_2^-$ addition (nmol L^{-1})
0.40	1.75	9.85	188.1
0.38	1.84	9.94	198.0
0.58	12.10	20.17	129.7
0.59	11.90	19.96	127.5
0.46	84.46	92.56	163.6
0.47	82.66	90.76	160.1
0.50	233.10	241.20	150.5
0.47	247.98	256.08	160.1

Statistical analysis—Diversity and evenness of the array archetypes were calculated using the Shannon-Wiener index:

$$H' = -\Sigma\, p_i \times \ln\, p_i$$

where H' is the diversity of each archetype and p_i is the proportional of each archetype to the total community signal; *amoA* community compositions at each depth were compared using analysis of variance (ANOVA) tests. Software packages JMP and Kaleidagraph were used for significance and ANOVA tests, and the Monte Carlo simulation was conducted in Matlab using the *normrnd* function to generate likely ammonia oxidation rates.

Results

The results capture the abundance, ammonia oxidation rate, and diversity of the ammonia-oxidizing community in a depth profile at BATS in December 2009. Nutrient profiles are shown in Figure 1A. Nitrate concentrations were undetectable shallower than 100 m but reached 21 μmol L^{-1} by 1000 m. The nitrite concentration reached 60 ± 8 nmol L^{-1} at 100 m, peaked at 64 ± 14 nmol L^{-1} at 120 m (the PNM), and decreased to undetectable levels by 300 m. Ammonium concentrations were variable (up to 26 nmol L^{-1}) throughout the upper 200 m and undetectable below 300 m.

Ammonia oxidation rates ranged from undetectable at the surface and 2000 m to 2.0 ± 0.1 nmol L^{-1} d^{-1} at 120 m (Fig. 1B). The depths with the highest rates (100 and 120 m) coincided with the PNM. Although supported by a small

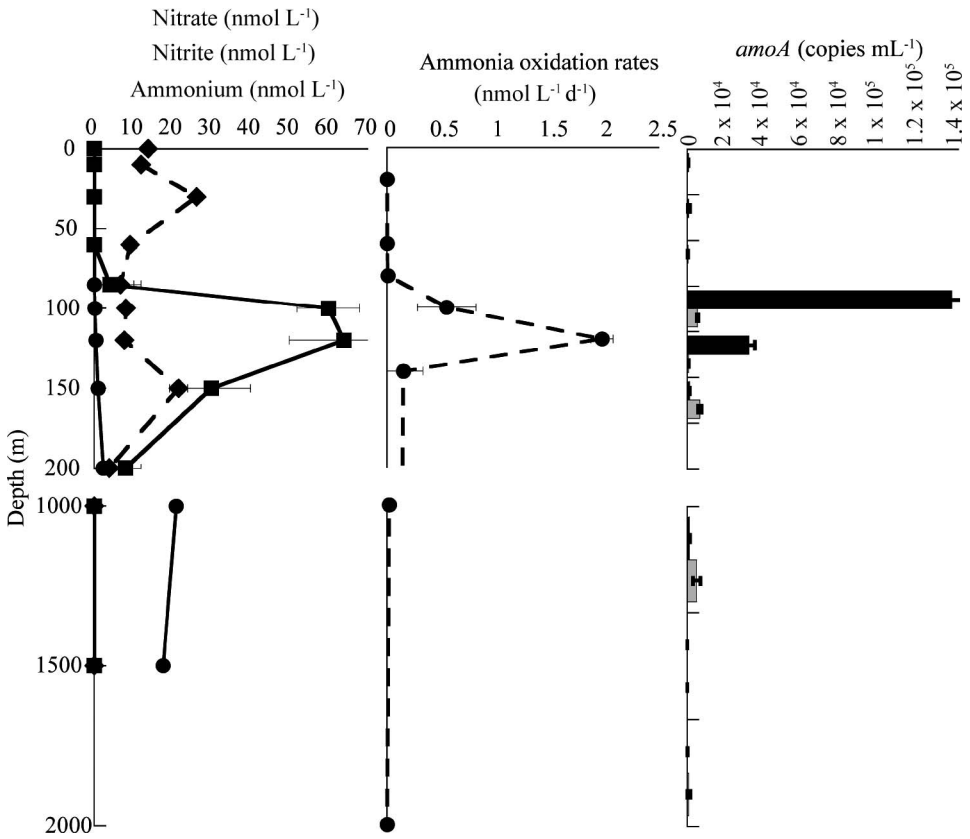

Fig. 1. Depth profiles for (A) nitrate (circles), nitrite (squares), and ammonium (diamonds) concentrations. For all, the error bars represent ± 1 SD of all samples. (B) Ammonia oxidation rates in nmol L^{-1} d^{-1}. Error bars are the range of duplicate measurements. (C) AOA and AOB *amoA* gene copy numbers, shown as copies mL^{-1}. Error bars are the SD of triplicate qPCR reactions.

number of measurements ($n = 8$), the relationship between ammonia oxidation rate and nitrite concentration was positive and significant ($R^2 = 0.63$, and $p < 0.05$ for a linear regression).

AOA *amoA* copies ranged from 204 ± 117 copies mL^{-1} at 2000 m to $1.37 \times 10^5 \pm 7.1 \times 10^3$ copies mL^{-1} at 100 m (Fig. 1C). The two depths (100 and 120 m) with the highest concentration of AOA *amoA* copies broadly coincided with the highest ammonia oxidation rates, although the rates were highest at 120 m and the gene copy numbers were highest at 100 m. The relationship between ammonia oxidation rates and AOA *amoA* copy number was not statistically significant ($p > 0.05$). AOB *amoA* were not detected from 20 to 80 m (Fig. 1C). AOA *amoA* gene copy numbers were two orders of magnitude higher than AOB gene copy numbers at 100 and 120 m, but at depths > 140 m, AOB *amoA* gene copy numbers exceeded AOA *amoA* by about fourfold.

The kinetic experiment revealed a Michaelis–Menten-type dependence (in which reaction rate increases with substrate concentration to asymptotically approach a maximum reaction rate, V_{max}) of ammonia oxidation rate on ammonium concentration at 100 m (Fig. 2, black filled circles). Ammonium substrate concentrations ($^{15}NH_4^+$ tracer addition plus ambient [NH_4^+]) ranged from ~ 10

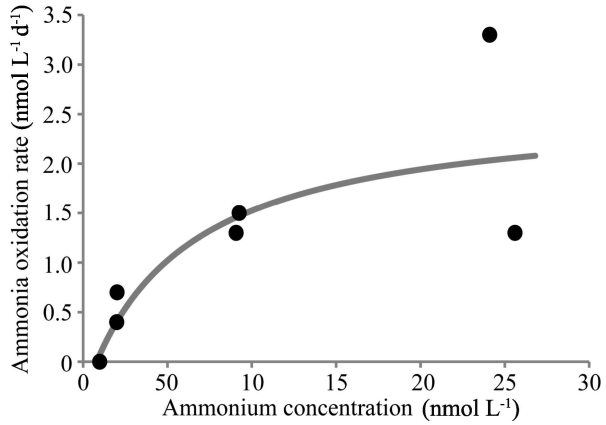

Fig. 2. The dependence of ammonia oxidation rate on substrate concentration at 100 m. Measured ammonia oxidation rates (nmol L^{-1} d^{-1}; filled black circles) are shown as a function of total ammonium concentration ($^{15}NH_4^+$ tracer addition + ambient ammonium concentration; nmol L^{-1}). A Michaelis–Menten function was fit to the data (gray line) using the mean values of K_m (65 ± 41 nmol L^{-1}) and V_{max} (2.6 ± 1.1 nmol L^{-1} d^{-1}) derived from a Eadie–Hofstee linearization ($R^2 = 0.71$, $n = 8$).

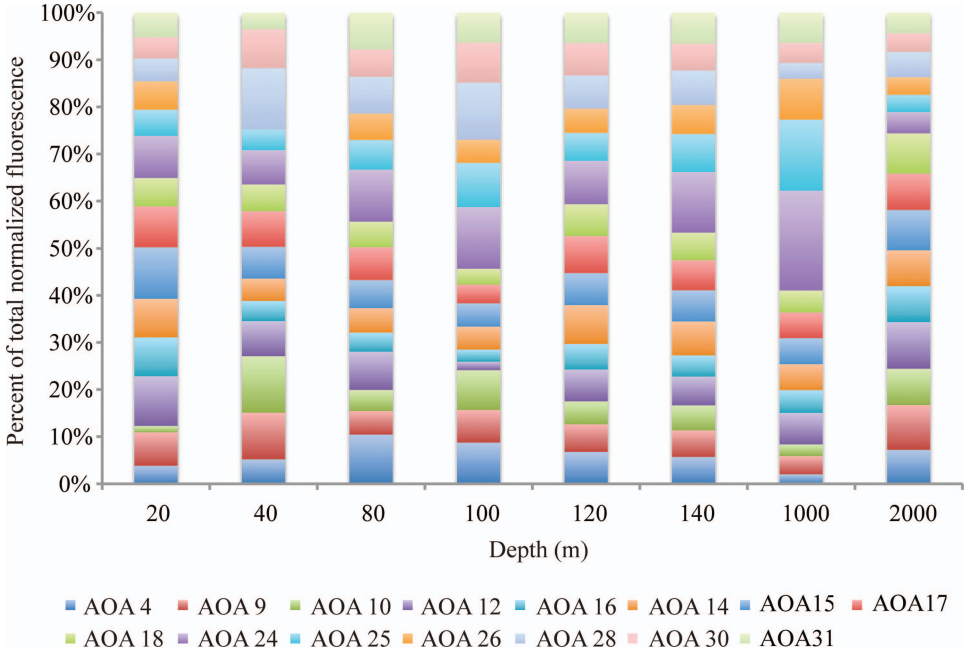

Fig. 3. The AOA *amoA* functional gene microarray community at eight depths. The community is represented by a stacked bar plot, showing the percentage of each probe's normalized Cy3 : C5 fluorescence ratio (FRn) to the sum of the community FRn. Only archetypes making up more than 5% of the total community at each depth are shown.

to 256 nmol L^{-1}, and the corresponding ammonia oxidation rates ranged from undetectable at the lowest substrate concentration to 3.3 nmol L^{-1} d^{-1} at the highest substrate concentration. The Eadie–Hofstee linearization generated estimates for K_m (the substrate concentration at half the maximum ammonia oxidation rate) and V_{max} (mean ± SD) of 65 ± 41 and 2.6 ± 1.1 nmol L^{-1} d^{-1}, respectively, from which the Michaelis–Menten fit (Fig. 2, gray curve) was derived ($R^2 = 0.71$; $n = 8$). This modeled Michaelis–Menten fit predicts ammonia oxidation rates for a 20–26 nmol L^{-1} substrate concentration (i.e., the $^{15}NH_4^+$ addition plus ambient ammonium concentration present in the depth profile incubations) ranging from 0.5 ± 0.4 to 0.7 ± 0.4 nmol L^{-1} d^{-1}, similar to the measured rate from the profile at 100 m of 0.6 ± 0.3 nmol L^{-1} d^{-1}.

AOA *amoA* community composition was relatively diverse (Shannon–Weiner diversity indices ranged from 3.16 to 3.36, $H_{max} = 3.40$) and even (Shannon–Weiner evenness values ranged from 0.93 to 0.99) across all eight depths (Fig. 3). The community at 120 m was significantly different from that at five other depths ($p < 0.05$) and not significantly different from that at 40 and 2000 m ($p = 0.15$). Archetype AOA24 had the highest Cy3 : Cy5 fluorescence ratio (all other probes were normalized to it) at 80 m through 1000 m but dropped to the 16th highest out of 30 at 2000 m (Fig. 4). The highest signal probe at 2000 m was AOA12, which was in the top five between 20 and 80 m and at 1000 m but not between 100 and 140 m.

Discussion

Ammonia oxidation rates—The highest ammonia oxidation rates and AOA *amoA* gene copy numbers (two and one orders of magnitude higher, respectively, than at all other depths) coincided with each other and were observed at 100 and 120 m (Fig. 1B,C), suggesting that AOA were responsible for most of the ammonia oxidation at BATS during December. The AOA : AOB *amoA* gene copy number ratio of ~ 4 at these depths supports this conclusion. This finding is not unexpected, as a number of recent studies have similarly observed the dominance of AOA over AOB in the open ocean (Beman et al. 2010; Santoro et al. 2010; Newell et al. 2011). It has been

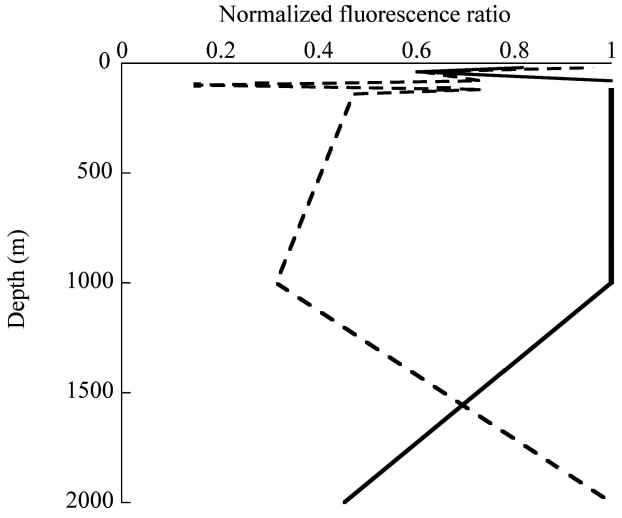

Fig. 4. Depth profile of the FRn of AOA24 (the archetype with the highest FRn down to 10.00 m) and AOA12 (the archetype with the highest FRn at 2000 m).

suggested that AOA outcompete AOB in oligotrophic environments due to their higher substrate affinity (Martens-Habbena et al. 2009). The K_m estimated from the natural assemblage here (65 ± 41 nmol L^{-1}), although uncertain, is similar to or even lower than that reported for *Nitrosopumilus martimus* (134 nmol L^{-1}; Martens-Habbena et al. 2009), indicating the high affinity for ammonium of the in situ community, possibly as a result of adaption to the oligotrophic conditions of the Sargasso Sea.

The ammonia oxidation rates measured in this study (up to 2.0 ± 0.1 nmol L^{-1} d^{-1}) are lower than those previously measured by similar tracer methods but of the same order of magnitude. The rates reported here are most similar to those from other open ocean environments: up to 10 nmol L^{-1} d^{-1} in the Atlantic (Clark et al. 2008), 3.2–21.6 nmol L^{-1} d^{-1} in the surface of the Arabian Sea (Newell et al. 2011), and 5–20 nmol L^{-1} d^{-1} in the Pacific off Baja California (Ward and Zafiriou 1988). Rates from more coastal environments are typically up to an order of magnitude higher, possibly because ambient ammonium concentrations tend to be higher in these regions: 9–210 nmol L^{-1} d^{-1} in the Central California Current (Santoro et al. 2010), up to 90 nmol L^{-1} d^{-1} in the Guaymas Basin (Beman et al. 2008), up to 40 nmol L^{-1} d^{-1} in the Carmen Basin (Beman et al. 2008), and 27.8–73.8 nmol L^{-1} d^{-1} in Monterey Bay (Ward 2005).

The PNM at BATS in December (120 m) coincided with the highest observed ammonia oxidation rate (2.0 ± 0.1 nmol L^{-1} d^{-1}), similar to the rate computed by Lipschultz (2001) on the basis of nitrite concentration changes. At this rate, it would take over a month to produce the PNM if it were maintained by ammonia oxidation alone. However, the relationship between rate and substrate concentration in Fig. 2 suggests that the rates measured in this study were below the potential maximum rates. Additionally, because we did not account for ammonium regeneration in the rate calculations, the calculated rates may underestimate the in situ rates.

The rates reported from the depth profile experiment occurred at ammonium concentrations ($^{15}NH_4^+$ tracer addition plus ambient [NH_4^+]) of 15 ± 4–36 ± 4 nmol L^{-1}. The kinetic experiment at 100 m showed a sixfold increase in the ammonia oxidation rate at a substrate concentration of 241 nmol L^{-1}. In situ ammonium concentrations at 100 and 120 m were much lower than the K_m (8.1 ± 0.2 and 7.7 ± 0.5 nmol L^{-1}, respectively). Although the enrichments were well above trace levels (59–70% ^{15}N), the total concentrations were still below the K_m, suggesting that the ammonia oxidation rates reported here might be a slight overestimate of the in situ rates. Since the measured rates are well below the potential rates implied by the kinetic experiment and given the high affinity of the natural assemblage for ammonium, a local increase in ammonium concentration may drive a rapid increase in the rate of its oxidation. A sixfold rate increase would produce the entire PNM in about a week, implying that short-term responses to ephemeral ammonium pulses might play an important role in forming and maintaining the PNM.

The other possible contributor to the formation of the PNM is excretion of NO_2^- by light-limited phytoplankton during the assimilation of NO_3^- (Lomas and Lipschultz 2006). At the time of these measurements, chlorophyll was very low at 100–120 m, and nitrate was barely detectable. Furthermore, measurements of the natural abundance N isotopic composition of flow cytometrically sorted populations of *Prochlorococcus*, *Synechococcus*, and eukaryotic phytoplankton at the base of the euphotic zone in December 2009 suggest that NH_4^+ was the dominant N source to all phytoplankton at this time (Fawcett 2012). These observations imply a very limited role for phytoplankton in the formation of the PNM in December, although light limitation could easily be a factor at this time of year. Thus, it seems likely that the longer turnover times inferred from our data reflect overall slower N transformation rates in the winter period than estimated by Lipschultz et al. (1996) in an annual study and by Beman et al. (2011) in May.

Ammonium concentrations were highest at 30 m (26.2 ± 1.4 nmol L^{-1}), but low AOA *amoA* and undetectable AOB *amoA* gene copy numbers, coupled with undetectable ammonia oxidation rates above 80 m, suggest that nitrification was not occurring within the euphotic zone in December. This is consistent with previous reports of undetectable euphotic zone nitrification during the period of spring mixing at BATS (February–March; Lomas et al. 2009). It is possible that photoinhibition prevented AOA from utilizing ammonium in the euphotic zone in December, although Lipschultz (2001) reported high euphotic nitrification rates for August, when upper water column light intensity would have been greater than in the early winter. It thus seems unlikely that photoinhibition is the primary reason that ammonia oxidation was not detected in the euphotic zone in December.

At the time of our sampling, the density structure of the entire euphotic zone was fairly homogenous, with a sharp pycnocline at 95–120 m (http://bats.bios.edu/data/735332.7185ctd.dat) that created a physical barrier between the euphotic zone and underlying deep waters. Under these conditions, the upward mixing of both newly nitrified nitrate and nitrifying organisms is impeded (Fawcett 2012), perhaps resulting in the observed lack of euphotic zone nitrification at BATS in December. Furthermore, as a direct consequence of the density-driven isolation of the euphotic zone from the subsurface nitrate supply, all phytoplankton were relying exclusively on ammonium at this time (Fawcett 2012). Any ammonia oxidizers in the euphotic zone may thus have been outcompeted by phytoplankton for the low levels of available ammonium, further limiting the potential for ammonia oxidation in surface waters. By contrast, in the late summer and early fall, the mixed layer at BATS is considerably shallower than the base of the euphotic zone (15–50 m) such that there is free exchange between subsurface waters and the lower euphotic zone (Fawcett 2012). One might expect euphotic zone nitrification to be more likely under these conditions, and, indeed, Lipschultz (2001) reported significant rates of nitrification in the euphotic zone in August, when the mixed layer had shoaled to < 20 m. Moreover, the density structure of the upper water column in the summer and fall allows subsurface nitrate to mix up into

the euphotic zone, where it is consumed by eukaryotic phytoplankton (Fawcett et al. 2011; Fawcett 2012), perhaps removing some of the competitive pressure between phytoplankton and ammonia oxidizers for ammonium. Thus, while ammonia oxidation did not occur in the euphotic zone in December, we predict that it may be important at other times of year, such as the late summer and early fall.

More speculatively, the annual nitrification rate implied by our December ammonia oxidation rates, integrated from the surface to 250 m (the average depth of spring overturning; Steinberg 2011), is $< 10\%$ of the annual nitrate supply flux (Jenkins et al. 1988; Spitzer and Jenkins 1989; McGillicuddy et al. 1998). While we recognize the many assumptions and caveats in this calculation, it nonetheless suggests that higher rates of ammonia oxidation must occur at other times of year and underlines the need for more studies at BATS to directly address the question of seasonal variability.

amoA abundance and community characterization—AOA *amoA* gene copy numbers were one to two orders of magnitude greater than AOB *amoA* gene copy numbers at depths < 120 m, suggesting that AOA were the dominant ammonia oxidizers. The total AOA *amoA* gene copy numbers were on the order of those observed by Agogue et al. (2008) for the eastern Atlantic at 30°N, although gene copy numbers at the PNM depth at BATS were an order of magnitude higher. The highest AOA *amoA* gene copy numbers at 100 m (1.3×10^5 copies L^{-1}) were very similar to the highest AOA *amoA* at 150 m in the Sargasso Sea (1×10^5 copies L^{-1}; Bouskill et al. 2009). Similarly, the greatest AOB *amoA* gene copy numbers at 100 m (6.5×10^3 copies L^{-1}) were the same order of magnitude as those reported for the Sargasso Sea at 150 m (1.5×10^3 copies L^{-1}; Bouskill et al. 2011). No AOB *amoA* copies were detected shallower than 100 m. This suggests the AOB may be more sensitive to light than AOA, although a recent culture study found a stronger light sensitivity for AOA (Merbt et al. 2012). Below the PNM, the AOB *amoA* gene copies outnumbered the AOA *amoA* by about fourfold. By contrast, Bouskill et al. (2011) reported greater AOA *amoA* than AOB *amoA* at all depths from the surface to 250 m (the greatest depth measured). In the present study, ammonium was undetectable below 300 m, so more work is necessary to understand the environmental drivers that allow AOB to outcompete AOA in the mesopelagic zone at BATS.

The AOA *amoA* functional gene microarray indicates an even community distribution (Fig. 3), but a single archetype (Probe AOA24, with the perfect-match sequence DS4_20, GenBank accession no. EF382456) maintained the highest normalized fluorescence ratio (FRn) from 80 through 1000 m (Fig. 4). DS4_20 was originally sequenced from the coral species *D. strigosa* in Bocas del Toro Panama (Beman et al. 2007). As corals prefer oligotrophic environments, perhaps similar to the oligotrophic Sargasso Sea, this finding supports the idea that certain archetypes flourish in similar environments around the world (Biller et al. 2012). AOA28 (perfect-match sequence DS2_6, GenBank accession no. EF382473) had the second-highest summed FRn across all of the arrays and was also originally sequenced from a coral (Beman et al. 2007). Another important archetype at six out of eight depths, AOA12 (perfect-match sequence R60-70_278, GenBank accession no. DQ534884) was sequenced from a sandy soil (Leininger et al. 2006), which is another environment characterized by low-nutrient conditions. Below the thermocline, AOA24 declined, while AOA12 had the highest FRn at 2000 m (Fig. 4). Although AOA1 represents the only marine AOA in culture (*N. maritimus*), it had one of the lowest FRn values from 20 to 1000 m, indicating that it was not a dominant contributor to the AOA community at BATS. This suggests that inferences made about AOA ecophysiology from *N. maritimus* cultures may not be representative of the in situ community.

Although the AOA community structure was fairly even, the community at 120 m (the depth of the PNM and the ammonia oxidation rate maximum) was significantly different from the community at five of the other depths (ANOVA; $p < 0.05$). AOA24 was still the dominant archetype at this depth. However, the probe with the second-highest FRn (AOA17) was not in the top five at 80, 100, or 140 m, suggesting that it might be responsible for the high rates at 120 m. The archetype probe AOA17 (JCS82-4, GenBank accession no. EU553403) represents cosmopolitan and versatile sequences that have been detected in the Black Sea, geothermal hot springs, and soil environments. The community at 2000 m was also different from that at the other depths, possibly because it was separated from the others by the permanent thermocline, which occurs just below 1000 m in the Sargasso Sea (Worthington 1976).

An AOA *amoA* microarray community analysis at 20 and 120 m from March 2009 at BATS, using the same probe set as presented here, was published previously (Bouskill et al. 2011). The March samples were collected during the onset of the spring bloom, in contrast to the oligotrophic season sampled in this study. Additionally, the Bouskill et al. (2011) study applied whole DNA to the array, whereas this study used AOA *amoA* PCR product. Of the three most important archetypes identified by Bouskill et al. (2011), archetypes AOA4 and AOA12 were also in the top 10 in this study (although AOA4 was not abundant at 20 m), but AOA9 was only in the top five at 20 m. However, the highest-signal archetype in this study—AOA24—was not a top archetype in March 2009, and the community was less even (0.71 and 0.69 on the Shannon–Weiner Evenness Index at 20 and 120 m, respectively) in March than in December 2009. The spring bloom appears to be associated with a much less even community dominated by a different combination of archetypes, with the most abundant archetype from December barely detectable in March. The greater evenness of the December community is probably significant and not due to the different method of target preparation; Ward and Bouskill (2011) showed that PCR and whole DNA targets give very similar results.

Taken as a whole, these data support the prevailing idea that archaea are the dominant ammonia oxidizers in the oligotrophic ocean, as the AOA greatly outnumber the

AOB, and the highest ammonia oxidation rates and AOA *amoA* gene copy numbers occur at similar depths. The depths with the highest rates and *amoA* gene copy numbers are also coincident with the PNM, suggesting that AOA are important contributors to the PNM, at least in December. However, below the PNM, AOB *amoA* outnumbered AOA *amoA* gene copy numbers, suggesting that in situ communities of both AOA and AOB have affinity for their primary substrate. The oligotrophic environment at BATS supports a consistently diverse AOA community whose evenness and composition vary between the most oligotrophic season and the winter and spring bloom period. Shifts in the community structure appear to be linked to seasonal biogeochemical changes, just as absolute rates of nitrification and the relative importance of nitrification as a source of regenerated nitrate in the euphotic zone may also vary on a seasonal basis.

Acknowledgments

We thank the captain and crew of the R/V *Atlantic Explorer*; the faculty and staff of the Bermuda Institute of Ocean Sciences, particularly Michael Lomas; and the University of California Davis Stable Isotope Laboratory. S.E.N. was funded by the National Science Foundation Graduate Research Fellowship and the National Science Foundation Postdoctoral Research Fellowship.

References

Agogue, H., M. Brink, J. Dinasquet, and G. J. Herndl. 2008. Major gradients in putatively nitrifying and non-nitrifying Archaea in the deep North Atlantic. Nature **456:** 788–791, doi:10.1038/nature07535

Beman, J. M., B. N. Popp, and C. A. Francis. 2008. Molecular and biogeochemical evidence for ammonia oxidation by marine Chrenarchaeota in the Gulf of California. ISME J. **2:** 429–441, doi:10.1038/ismej.2007.118

———, K. J. Roberts, L. Wegley, F. Rohwer, and C. A. Francis. 2007. Distribution and diversity of Archaeal ammonia monooxygenase genes associated with corals. Appl. Environ. Microbiol. **73:** 5642–5647, doi:10.1128/AEM.00461-07

———, R. Sachdeva, and J. A. Fuhrman. 2010. Population ecology of nitrifying Archaea and Bacteria in the Southern California Bight. Environ. Microbiol. **12:** 1282–1292, doi:10.1111/j.1462-2920.2010.02172.x

———, and others. 2011. Global declines in oceanic nitrification rates as a consequence of ocean acidification. Proc. Natl. Acad. Sci. USA **108:** 208–213, doi:10.1073/pnas.1011053108

Bernhard, A. E., J. Tucker, A. E. Giblin, and D. A. Stahl. 2007. Functionally distinct communities of ammonia-oxidizing bacteria along an estuarine salinity gradient. Environ. Microbiol. **9:** 1439–1447, doi:10.1111/j.1462-2920.2007.01260.x

———, Z. C. Landry, A. Blevins, J. R. de la Torre, A. E. Giblin, and D. A. Stahl. 2010. Abundance of ammonia-oxidizing *archaea* and *bacteria* along an estuarine salinity gradient in relationship to potential nitrification rates. Appl. Environ. Microbiol. **76:** 1285-1289, doi:10.1128/AEM.02018-09

Biller, S. J., A. C. Mosier, G. F. Wells, and C. A. Francis. 2012. Global biodiversity of aquatic ammonia-oxidizing archaea is partitioned by habitat. Front. Aquat. Microbiol. **3:** 252.

Bouskill, N. J., D. Eveillard, D. Chien, A. Jayakumar, and B. B. Ward. 2011. Environmental factors determining ammonia-oxidizing organism distribution and diversity in marine environments. Environ. Microbiol. **14:** 714–729, doi:10.1111/j.1462-2920.2011.02623.x

Braman, R. S., and S. A. Hendrix. 1989. Nanogram nitrite and nitrate determination in environmental and biological materials by vanadium (III) reduction with chemiluminescence detection. Anal. Chem. **61:** 2715–2718, doi:10.1021/ac00199a007

Bulow, S. E., C. A. Francis, G. A. Jackson, and B. B. Ward. 2008. Sediment denitrifier community composition and nirS gene expression investigated with functional gene microarrays. Environ. Microbiol. **10:** 3057–3069, doi:10.1111/j.1462-2920.2008.01765.x

Church, M. J., B. Wai, D. M. Karl, and E. F. DeLong. 2010. Abundances of crenarchaeal *amoA* genes and transcripts in the Pacific Ocean. Environ. Microbiol. **12:** 679–688, doi:10.1111/j.1462-2920.2009.02108.x

Clark, D. R., A. P. Rees, and I. Joint. 2008. Ammonium regeneration and nitrification rates in the oligotrophic Atlantic Ocean: Implications for new production estimates. Limnol. Oceanogr. **53:** 52–62, doi:10.4319/lo.2008.53.1.0052

———, ———, and ———. 2008. Ammonium regeneration and nitrification rates in the oligotrophic Atlantic Ocean: Implications for new production estimates. Limnol. Oceanogr. **53:** 52–62, doi:10.4319/lo.2008.53.1.0052

Dang, H., X. Zhang, J. Sun, T. Li, Z. Zhang, and G. Yang. 2008. Diversity and spatial distribution of sediment ammonia-oxidizing crenarchaeota in response to estuarine and environmental gradients in the Changjiang Estuary and East China Sea. Microbiology **154:** 2084–2095, doi:10.1099/mic.0.2007/013581-0

———, and others. 2009. Diversity and distribution of sediment nirS-encoding bacterial assemblages in response to environmental gradients in the eutrophied Jiaozhou Bay, China. Microb. Ecol. **58:** 161–169, doi:10.1007/s00248-008-9469-5

———, and ———. 2013. Environment-dependent distribution of sediment nifH-harboring microbiota in the northern South China Sea. Appl. Environ. Microbiol. **79:** 121–132, doi:10.1128/AEM.01889-12

Fawcett, S. E. 2012. Nitrate assimilation by eukaryotic phytoplankton as a central characteristic of ocean productivity. Ph.D. thesis. Princeton Univ.

———, M. W. Lomas, B. B. Ward, and D. M. Sigman. 2011. Assimilation of upwelled nitrate by small eukaryotes in the Sargasso Sea. Nat. Geosci. **4:** 717–722, doi:10.1038/ngeo1265

Francis, C. A., G. D. O'Mullan, and B. B. Ward. 2003. Diversity of ammonia monooxygenase (*amoA*) genes across environmental gradients in Chesapeake Bay sediments. Geobiology **1:** 129–140, doi:10.1046/j.1472-4669.2003.00010.x

———, K. J. Roberts, M. J. Beman, A. E. Santoro, and B. B. Oakley. 2005. Ubiquity and diversity of ammonia-oxidizing archaea in water columns and sediments of the ocean. Proc. Natl. Acad. Sci. USA **102:** 14683–14688, doi:10.1073/pnas.0506625102

Garside, C. 1982. A chemiluminescent technique for the determination of nanomolar concentrations of nitrate and nitrite in seawater. Mar. Chem. **11:** 159–167, doi:10.1016/0304-4203(82)90039-1

Gruber, N., and J. L. Sarmiento. 1997. Global patterns of marine nitrogen fixation and denitrification. Glob. Biogeochem. Cycles **11:** 235–266, doi:10.1029/97GB00077

Holmes, R. M., A. Aminot, R. Kerouel, B. A. Hooker, and B. J. Peterson. 1999. A simple and precise method for measuring ammonium in marine and freshwater ecosystems. Can. J. Fish. Aquat. Sci. **56:** 1801–1808.

Jenkins, W. J., D. J. Webb, L. Merlivat, and W. Roether. 1988. The use of anthropogenic tritium and helium-3 to study subtropical gyre ventilation and circulation [and discussion]. Phil. Trans. Roy. Soc. London. Ser. A. **325:** 43–61, doi:10.1098/rsta.1988.0041

Kiefer, D., R. Olson, and O. Holm-Hansen. 1976. Another look at the nitrite and chlorophyll max in the central North Pacific. Deep-Sea Res. I **23:** 1199–1208.

Konneke, M., A. E. Berhnard, J. R. de la Torre, C. B. Walker, J. B. Waterbury, and D. A. Stahl. 2005. Isolation of an autotrophic ammonia-oxidizing marine archaeon. Nature **437:** 543–546, doi:10.1038/nature03911

Leininger, S., and others. 2006. Archaea predominate among ammonia-oxidizing prokaryotes in soils. Nature **442:** 806–809, doi:10.1038/nature04983

Lipschultz, F. 2001. A time series assessment of the nitrogen cycle in the Sargasso Sea. Deep-Sea Res. II **48:** 1897–1924, doi:10.1016/S0967-0645(00)00168-5

———, O. C. Zafiriou, and L. A. Ball. 1996. Seasonal fluctuations of nitrite concentrations in the deep oligotrophic ocean. Deep-Sea Res. II **43:** 403–419, doi:10.1016/0967-0645(96)00003-3

Lomas, M. W., N. R. Bates, R. J. Johnson, A. H. Knap, D. K. Steinberg, and C. A. Carlson. In press. Two decades and counting: 24-years of sustained open ocean biogeochemical measurements in the Sargasso Sea. Deep-Sea Res. II, doi:10.1016/j.dsr2.2013.01.008

———, and F. Lipschultz. 2006. Forming the primary nitrite maximum: Nitrifiers or phytoplankton? Limnol. Oceanogr. **51:** 2453–2467, doi:10.4319/lo.2006.51.5.2453

———, ———, D. M. Nelson, J. W. Krause, and N. R. Bates. 2009. Biogeochemical responses to late-winter storms in the Sargasso Sea, I—Pulses of primary and new production. Deep-Sea Res. **56:** 843–886, doi:10.1016/j.dsr.2008.09.002

Mackey, K. R. M., L. Bristow, D. R. Parks, M. A. Altabet, A. F. Post, and A. Paytan. 2011. The influence of light on nitrogen cycling and the primary nitrite maximum in a seasonally stratified sea. Prog. Oceanogr. **91:** 545–560, doi:10.1016/j.pocean.2011.09.001

Martens-Habbena, W., P. M. Berube, H. Urakawa, J. R. de la Torre, and D. A. Stahl. 2009. Ammonia oxidation kinetics determine niche separation of nitrifying Archaea and Bacteria. Nature **461:** 976–981, doi:10.1038/nature08465

Martin, A. P., and P. Pondaven. 2006. New primary production and nitrification in the western subtropical North Atlantic: A modeling study. Glob. Biogeochem. Cycles **20:** GB4014, doi:10.1029/2005GB002608

McGillicuddy, D. J., and others. 1998. Influence of mesoscale eddies on new production in the Sargasso Sea. Nature **394:** 263–265, doi:10.1038/28367

McIlvin, M. R., and M. A. Altabet. 2005. Chemical conversion of nitrate and nitrite to nitrous oxide for nitrogen and oxygen isotopic analysis in freshwater and seawater. Anal. Chem. **77:** 5589–5595, doi:10.1021/ac050528s

Menzel, D. W., and J. H. Ryther. 1960. The annual cycle of primary production in the Sargasso Sea off Bermuda. Deep-Sea Res. **6:** 351–367.

Merbt, S. N., D. A. Stahl, E. O. Casamayor, E. Martí, G. W. Nicol, and J. I. Prosser. 2012. Differential photoinhibition of bacterial and archaeal ammonia oxidation. FEMS Microbiol. Lett. **327:** 41–46, doi:10.1111/j.1574-6968.2011.02457.x

Mincer, T. J., M. J. Church, L. T. Taylor, C. Preston, D. M. Karl, and E. F. DeLong. 2007. Quantitative distribution of presumptive archaeal and bacterial nitrifiers in Monterey Bay and the North Pacific Subtropical Gyre. Environ. Microbiol. **9:** 1162–1175, doi:10.1111/j.1462-2920.2007.01239.x

Newell, S. E., A. R. Babbin, A. Jayakumar, and B. B. Ward. 2011. Ammonia oxidation rates and nitrification in the Arabian Sea. Glob. Biogeochem. Cycles **25:** GB4016, doi:10.1029/2010GB003940

Rotthauwe, J. H., K. P. Witzel, and W. Liesack. 1997. The ammonia monooxygenase structural gene amoA as a functional marker: molecular fine-scale analysis of natural ammonia-oxidizing populations. Appl. Environ. Microbiol. **63:** 4704–4712.

Santoro, A. E., K. L. Casciotti, and C. A. Francis. 2010. Activity, abundance and diversity of nitrifying archaea and bacteria in the central California Current. Environ. Microbiol. **12:** 1989–2006, doi:10.1111/j.1462-2920.2010.02205.x

Smith, C. J., D. B. Nedwell, L. F. Dong, and A. M. Osbourn. 2007. Diversity and abundance of nitrate reductase genes (*narG* and *napA*), nitrite reductase genes (*nirS* and *nrfA*), and their transcripts in estuarine sediments. Appl. Environ. Microbiol. **73:** 3612–3622, doi:10.1128/AEM.02894-06

Spitzer, W. S., and W. J. Jenkins. 1989. Rates of vertical mixing, gas exchange and new production: Estimates from seasonal gas cycles in the upper ocean near Bermuda. J. Mar. Res. **47:** 169–196, doi:10.1357/002224089785076370

Steinberg, D. K., C. A. Carlson, N. R. Bates, R. J. Johnson, A. F. Michaels, and A. H. Knap. 2001. Overview of the US JGOFS Bermuda Atlantic Time-series Study (BATS): A decade-scale look at ocean biology and biogeochemistry. Deep-Sea Res. II **48:** 1405–1447, doi:10.1016/S0967-0645(00)00148-X

Strickland, J. D. H., and T. R. Parsons. 1968. A practical handbook of seawater analysis. Bulletin of the Fisheries Research Board of Canada. Ottawa.

Ward, B. B. 2005. Temporal variability in nitrification rates and related biogeochemical factors in Monterey Bay, California, USA. Mar. Ecol. Prog. Ser. **292**: 97–109, doi:10.3354/meps292097

———, and N. J. Bouskill. 2011. The utility of functional gene arrays for assessing community composition, relative abundance, and distribution of ammonia-oxidizing bacteria and archaea. Methods Enzymol. **496:** 373–396, doi:10.1016/B978-0-12-386489-5.00015-4

———, D. Eveillard, J. D. Kirshtein, J. D. Nelson, M. A. Voytek, and G. A. Jackson. 2007. Ammonia-oxidizing bacterial community composition in estuarine and oceanic environments assessed using a functional gene microarray. Environ. Microbiol. **9:** 2522–2538, doi:10.1111/j.1462-2920.2007.01371.x

———, and K. A. Kilpatrick. 1990. Relationship between substrate concentration and oxidation of ammonium and methane in a stratified water column. Cont. Shelf Res. **10:** 1193–1208, doi:10.1016/0278-4343(90)90016-F

———, and O. C. Zafiriou. 1988. Nitrification and nitric oxide in the oxygen minimum of the eastern tropical North Pacific. Deep-Sea Res. **35:** 1127–1142.

———, R. J. Olson, and M. J. Perry. 1982. Microbial nitrification rates in the primary nitrite maximum off Southern California. Deep-Sea Res. **29:** 247–255.

Worthington, L. V. 1976. On the North Atlantic circulation. The Johns Hopkins Oceanographic Studies 6. Baltimore.

Wuchter, C., and others. 2006. Archaeal nitrification in the ocean. Proc. Natl. Acad. Sci. USA **103:** 12317–12322, doi:10.1073/pnas.0600756103

Yool, A., A. P. Martin, C. Fernandez, and D. R. Clark. 2007. The significance of nitrification for oceanic new production. Nature **447:** 999–1002, doi:10.1038/nature05885

Associate editor: Bo Thamdrup

Received: 03 September 2012
Accepted: 25 March 2013
Amended: 10 April 2013